HtrA2/Omi-immunoreactive intraneuronal inclusions in the anterior horn of patients with sporadic and Cu/Zn superoxide dismutase (SOD1) mutant amyotrophic lateral sclerosis

Y. Kawamoto*†, H. Ito*, Y. Kobayashi*, Y. Suzuki‡, I. Akiguchi§, H. Fujimura¶, S. Sakoda**, H. Kusaka††, A. Hirano‡‡ and R. Takahashi*

*Department of Neurology, Faculty of Medicine, Kyoto University, Kyoto, †Department of Neurology, Seijinkai Shimizu Hospital, Kyoto, ‡Department of Degenerative Neurological Diseases, National Institute of Neuroscience, National Center of Neurology and Psychiatry, Tokyo, §Department of Neurology, Center of Neurological and Cerebrovascular Diseases, Koseikai Takeda Hospital, Kyoto, ¶Department of Neurology, National Hospital Organization Toneyama National Hospital, Osaka, **Department of Neurology, D-4, Osaka University Graduate School of Medicine, Osaka, ††Department of Neurology, Kansai Medical University, Osaka, Japan, and ‡‡Division of Neuropathology, Department of Pathology, Montefiore Medical Center, New York, USA

HtrA2/Omi-immunoreactive intraneuronal inclusions in the anterior horn of patients with sporadic and Cu/Zn superoxide dismutase (SOD1) mutant amyotrophic lateral sclerosis

Aims: HtrA2/Omi is a mitochondrial serine protease that promotes the apoptotic processes, but the relationship between HtrA2/Omi and amyotrophic lateral sclerosis (ALS) is still unknown. The purpose of the present study was to determine whether abnormal expression of HtrA2/Omi occurs in patients with ALS. **Methods:** We prepared autopsied spinal cord tissues from 7 control subjects, 11 patients with sporadic ALS (SALS) and 4 patients with Cu/Zn superoxide dismutase (SOD1)-related familial ALS (FALS). We then performed immunohistochemical studies on HtrA2/Omi using formalin-fixed, paraffin-embedded sections from all of the cases. **Results:** In the control subjects, the anterior horn cells were mildly to moderately immunostained with HtrA2/Omi. In the patients with SALS, strong HtrA2/Omi immunoreactivity was found in some skein-like inclusions and round hyaline inclusions as well as many spheroids, but Bunina bodies were immunonegative for HtrA2/Omi. In the patients with SOD1-related FALS, Lewy body-like hyaline inclusions were observed in three cases and conglomerate inclusions were observed in the remaining case, and both types of inclusions were intensely immunopositive for HtrA2/Omi. **Conclusions:** These results suggest that abnormal accumulations of HtrA2/Omi may occur in several types of motor neuronal inclusions in the anterior horn from SALS and SOD1-linked FALS cases, and that HtrA2/Omi may be associated with the pathogenesis of both types of ALS.

Keywords: amyotrophic lateral sclerosis, conglomerate inclusions, HtrA2/Omi, Lewy body-like hyaline inclusions, round hyaline inclusions, skein-like inclusions

---

Correspondence: Yasuhiro Kawamoto, Department of Neurology, Faculty of Medicine, Kyoto University, 54 Shogoin-Kawaharacho, Sakyoku, Kyoto 606-8507, Japan. Tel: +81-75-751-3766; Fax: +81-75-751-3265; E-mail: kawamoto@kuhp.kyoto-u.ac.jp

Introduction

Amyotrophic lateral sclerosis (ALS) is a fatal progressive neurodegenerative disease that is characterized by

331

degeneration of both upper and lower motor neurones. Although most cases of ALS are sporadic, about 10% of patients with ALS are familial forms [1]. Rosen and colleagues demonstrated that several missense mutations in the gene encoding Cu/Zn superoxide dismutase (SOD1) were associated with familial ALS (FALS) [2]. To date, over 120 different SOD1 mutations have been reported, and approximately 20% of FALS is caused by mutations in the SOD1 gene [1]. Lewy body-like hyaline inclusions (LBHIs), which were initially described in the cytoplasm of remaining anterior horn cells by Hirano and co-workers [3], are strongly immunopositive for SOD1 [4], and motor neuronal LBHIs are a hallmark of SOD1-related FALS. In addition, mutant SOD1 transgenic (mSOD1-Tg) mice replicate the clinical and pathological features of human illness, and are now well-established mouse models for FALS [1,5].

Mitochondria play an important role in the process of apoptotic cell death. During various apoptotic stimuli, cytochrome c is released from the mitochondria, and binds to apoptotic protease activating factor-1, thus resulting in the activation of caspase-9 [6,7]. Activated caspase-9 subsequently promotes the activation of caspase-3 and other caspases, leading to apoptotic cell death [6,7]. The inhibitor of apoptosis proteins (IAPs) have the ability to regulate apoptosis, and some IAP family proteins, such as X chromosome-linked IAP (XIAP), bind to and directly inhibit selected caspases [8–10]. HtrA2/Omi was identified as a mitochondrial serine protease that interacts with IAPs and contributes to the progression of apoptosis [11–14]. HtrA2/Omi is released from the mitochondrial intermembrane space into the cytosol upon receiving various apoptotic stimuli, and this released HtrA2/Omi induces apoptotic cell death by binding to IAPs, including XIAP, and blocking their caspase-inhibitory activities [11–16]. HtrA2/Omi also enhances caspase activation by inducing permeabilization of the outer mitochondrial membrane, which leads to the release of cytochrome c [17].

Caspase-9 is activated in surviving spinal motor neurones of mSOD1-Tg mice [18] and patients with sporadic ALS (SALS) [19], and XIAP is able to attenuate disease progression of mSOD1-Tg mice by inhibiting caspase-9 activity [19]. These data suggest that caspase-9 may play a crucial role in the pathogenesis of ALS. HtrA2/Omi is associated with the activation of caspase-9, but the relationship between HtrA2/Omi and ALS is still unknown. To elucidate the role of HtrA2/Omi

in patients with ALS, we performed immunohistochemical studies on HtrA2/Omi using autopsied spinal cord tissues from patients with ALS. We found strong HtrA2/Omi immunoreactivity in several types of motor neuronal inclusions in the anterior horn from both SALS and FALS cases.

Materials and methods

Tissue preparation

We studied spinal cords from 7 patients with other neurological or non-neurological disorders without spinal cord involvement (age range, 36–75 years; mean, 59.1 years; 4 men and 3 women), 11 patients with SALS (age range, 50–82 years; mean, 63.5 years; 7 men and 4 women), and 4 patients with FALS (age range, 43–64 years; mean, 49.3 years; 3 men and 1 woman). The clinical profiles from all cases are summarized in Table 1. Paraffin-embedded blocks were obtained from the formalin-fixed spinal cords of all cases, and these blocks were cut into 6-µm-thick sections on a microtome. Paraffin-embedded sections were deparaffinized in xylene, followed by rehydration in a decreasing concentration of ethanol solutions. For routine pathological examination, the deparaffinized sections from all blocks were stained with haematoxylin and eosin, Klüver-Barrera and modified Bielschowsky methods. Neuronal degeneration was restricted to the upper and lower motor neuronal systems in the 10 patients with SALS, and the remaining SALS patient, whose survival was prolonged with an artificial respirator, showed the neuronal loss and marked astrogliosis in various regions, including the cerebral neocortex, hippocampus, basal ganglia, thalamus, substantia nigra and spinal anterior horn. Bunina bodies were found in all the SALS cases. All of the patients with FALS were confirmed to have an abnormality in the gene encoding SOD1, and LBHIs were observed in the three cases (Ala4Val, Ile112Thr and a 2-base pair deletion at codon 126) and conglomerate inclusions (CIs) were observed in the remaining case (Ile113Thr). Because the patients with non-ALS showed no clinical symptoms or signs of spinal cord lesions, and no histological abnormalities were detected in any of the spinal cord sections from the non-ALS cases, these cases served as normal controls. The use of human materials was in agreement with the ethical guideline set by Kyoto University.

Table 1. Clinical profiles of all cases

Case	Age (year)/sex	Diagnosis	Duration of illness (month)/post mortem delay (h)
Control 1	52/M	Cerebral infarction	NA/UD
Control 2	51/F	Epilepsy	NA/11.5
Control 3	53/F	Myotonic dystrophy	NA/4.0
Control 4	74/F	Cerebral infarction	NA/UD
Control 5	73/M	Cerebral infarction	NA/2.3
Control 6	36/M	Hepatic encephalopathy	NA/2.7
Control 7	75/M	Chronic lymphocytic leukaemia	NA/2.5
SALS 1	68/M	SALS	48/1.0
SALS 2	50/M	SALS	84/3.7
SALS 3	63/M	SALS	21/1.5
SALS 4	60/F	SALS	40/2.5
SALS 5	56/F	SALS	20/10.5
SALS 6	58/F	SALS	42/3.5
SALS 7	64/M	SALS	26/3.0
SALS 8	71/F	SALS	19/3.3
SALS 9	62/M	SALS	26/1.3
SALS 10	82/M	SALS	15/1.4
SALS 11	65/M	SALS with respirator support	132/5.0
FALS 1	46/M	FALS (Ala4Val)	8/UD
FALS 2	43/M	FALS (Ile112Thr)	17/2.7
FALS 3	44/F	FALS (2bp del 126)	24/5.0
FALS 4	64/M	FALS (Ile113Thr)	6/5.0

M, male; F, female; NA, not applicable; UD, undetermined; SALS, sporadic amyotrophic lateral sclerosis; FALS, familial amyotrophic lateral sclerosis.

Patients with FALS

Familial ALS 1 is a member of the American 'C' family with an Ala4Val mutation in the SOD1 gene, and showed pathological upper and lower motor neuronal degeneration with posterior column and spinocerebellar tract involvement [3]. In addition, neuronal cytoplasmic LBHIs and cord-like swollen neurites were observed in the anterior horn [3], and these structures were demonstrated to be intensely immunostained with SOD1 [4].

Familial ALS 2 is a case with an Ile112Thr mutation in the SOD1 gene. Its neuropathological findings were similar to those of FALS 1, and neuronal degeneration was observed in the posterior column and spinocerebellar tracts as well as the upper and lower motor neurones. Many LBHIs were found in the somata and processes of the remaining anterior horn cells, and these LBHIs were strongly immunopositive for SOD1 (data not published).

Familial ALS 3 is a case with a 2-base pair deletion in exon 5 of the SOD1 gene (TTG → **G at Leu[126]) [20]. Although the posterior column was spared, many LBHIs were observed in the surviving spinal motor neurones [20]. These LBHIs were initially reported to be immunonegative for SOD1 [20], but were verified to be

immunolabelled with SOD1 using a different anti-SOD1 antibody [21].

Familial ALS 4 is a case with an Ile113Thr mutation in the SOD1 gene. In accordance with other FALS patients with an Ile113Thr mutation in the SOD1 gene [22–24], this patient showed marked neurofilamentous pathology, and many CIs were found in the remaining anterior horn cells (data not published).

Immunohistochemistry

To examine the immunohistochemical localization of HtrA2/Omi in normal and diseased spinal cords, we used an anti-HtrA2/Omi antiserum raised by immunizing rabbits with *Escherichia coli* expressing the C-terminal His6-tagged mature form of human HtrA2/Omi protein [11]. We have already confirmed that the antiserum could specifically recognize the mature form of HtrA2/Omi in human brains in the previous manuscript [25]. Deparaffinized sections were pretreated with 0.3% hydrogen peroxide (Santoku, Tokyo, Japan) in 0.1 M phosphate-buffered saline (PBS) for 30 min at room temperature to inhibit endogenous peroxidase activity. After washing with 0.1 M PBS, the sections were blocked with 0.1 M PBS

with 3% skim milk for 2 h at room temperature. After rinsing with 0.1 M PBS, the anti-HtrA2/Omi antiserum diluted in 0.1 M PBS (1:200) was applied onto the sections, and the sections were incubated overnight at room temperature or at 4°C in a humidified chamber. After washing with 0.1 M PBS, the sections were reacted with a biotinylated anti-rabbit IgG (Vector Laboratories, Burlingame, CA, USA) diluted in 0.1 M PBS (1:200) for 1 h at room temperature, followed by incubation with an avidin-biotin-peroxidase complex kit (Vector Laboratories) diluted in 0.1 M PBS (1:400) for 1 h at room temperature. After rinsing with 0.1 M PBS and then 0.05 M Tris-HCl (pH 7.6), the sections were developed in a colorizing solution containing 0.02% diaminobenzidine tetrahydrochloride (Dojin, Kumamoto, Japan), 0.6% ammonium nickel (II) sulphate (Wako, Osaka, Japan) and 0.005% hydrogen peroxide in 0.05 M Tris-HCl (pH 7.6) for 10 min at room temperature.

To investigate the relationship between HtrA2/Omi and several types of motor neuronal inclusions in the anterior horn from the SALS and FALS cases, some haematoxylin and eosin stained sections with motor neuronal inclusions were photographed, decolorized with 70% ethanol, and then immunostained with the anti-HtrA2/Omi antiserum using the avidin-biotin-peroxidase complex method described above.

As a negative immunohistochemical control, some sections were incubated with a pre-immune rabbit serum, and no specific immunopositive staining was detected in the sections treated thus (data not shown).

Double immunofluorescence staining

To investigate the relationship between HtrA2/Omi and ubiquitin, TAR DNA-binding protein of 43 kDa (TDP-43), or SOD1, we performed double-labelling immunohistochemistry using the anti-HtrA2/Omi antiserum and a goat polyclonal anti-ubiquitin antibody (sc-222, Santa Cruz Biotechnology, Santa Cruz, CA, USA), a mouse monoclonal anti-phospholylated TDP-43 antibody (Cosmo Bio, Tokyo, Japan) or a goat polyclonal anti-SOD1 antibody (sc-111, Santa Cruz Biotechnology). We applied the combination of the anti-HtrA2/Omi antiserum (1:200) plus the anti-ubiquitin antibody (1:500) or the anti-phospholylated TDP-43 antibody (1:2000) in some sections from the SALS cases, and that of the anti-HtrA2/Omi antiserum (1:200) plus the anti-SOD1 antibody (1:100) in some sections from the FALS cases. After incu-

bation of the sections with the primary antibodies overnight at room temperature or at 4°C, these sections were washed with 0.01 M PBS, and then reacted with secondary antibodies consisting of a tetramethylrhodamine-conjugated swine anti-rabbit IgG (DakoCytomation, Glostrup, Denmark) and a fluorescein isothiocyanate-conjugated swine anti-goat IgG (Biosource, Camarillo, CA, USA) or a fluorescein isothiocyanate-conjugated goat anti-mouse IgG (Bethyl Laboratories, Montgomery, TX, USA). After rinsing with 0.01 M PBS, the slides were coverslipped with Vectashield (Vector Laboratories), and were then viewed using a fluorescence microscope system (BZ-9000, Keyence, Osaka, Japan).

Semiquantitative assessment of HtrA2/Omi-immunopositive round hyaline inclusions (RHIs) and LBHIs

To evaluate the proportions of HtrA2/Omi-immunopositive RHIs and LBHIs, we prepared double-immunostained sections with HtrA2/Omi and ubiquitin from the 10 SALS cases (SALS 1-10) and those with HtrA2/Omi and SOD1 from three FALS cases (Ala4Val, Ile112Thr and a 2-base pair deletion at codon 126). After counting the ubiquitin-immunopositive RHIs and SOD1-immunopositive LBHIs in the anterior horns, we counted the double-immunolabelled RHIs and LBHIs in the same areas, and then calculated the average percentages of HtrA2/Omi-immunoreactive RHIs and LBHIs, respectively.

Characterization of the primary antiserum

The specificity of the anti-HtrA2/Omi antiserum was verified by Western blotting. Fresh tissues were obtained from the lumbar spinal cords of an autopsied normal subject (52-year-old man), an autopsied SALS case (60-year-old woman) and an autopsied SOD1-related FALS case (43-year-old man). These materials were homogenized in three volumes of ice-cold 10 mM PBS containing 1% Nonidet P-40 (Nacalai Tesque, Kyoto, Japan), 0.5% sodium deoxycholate (Difco, Detroit, MI, USA), 0.1% sodium dodecyl sulphate (Nacalai Tesque), 0.01% phenylmethylsulfonyl fluoride (Nacalai Tesque), 3% aprotinin (Sigma, St Louis, MO, USA) and 1 mM sodium orthovanadate (Sigma). The homogenates were then centrifuged at 25 000 g for 15 min at 4°C, and the supernatants were then mixed with an equivalent volume of electrophoresis sample

buffer containing 10% glycerol (Nacalai Tesque), 2% sodium dodecyl sulphate, 5% 2-mercaptoethanol (Nacalai Tesque) and 0.00125% bromophenol blue (Nacalai Tesque) in 62.5 mM Tris-HCl (pH 6.8). All of the samples were heated for 3 min at 100°C, and then cooled to room temperature. A 10-μl aliquot of the sample was loaded onto each lane of Mini-Protean II Ready Gels J (Bio-Rad, Hercules, CA, USA), electrophoresed at a constant voltage of 200 V, and then transferred onto polyvinylidene difluoride membranes (Bio-Rad) at a constant voltage of 100 V. After blocking the non-specific reactions with 3% skim milk plus normal goat serum in 25 mM Tris-buffered saline (TBS), the membranes were incubated with the anti-HtrA2/ Omi antiserum (1:2000) in 25 mM TBS plus 3% skim milk for 4 h at room temperature. After washing with 25 mM TBS containing 0.1% Tween-20 (Bio-Rad), the membranes were reacted with an alkaline phosphatase-labelled anti-rabbit IgG (Vector Laboratories, 1:1000) in 25 mM TBS with 3% skim milk for 1 h at room temperature. After rinsing with 25 mM TBS containing 0.1% Tween-20, the primary antibodies were visualized using a 5-bromo-4-chloro-3-indolyl phosphate/nitroblue tetrazolium kit (Nacalai Tesque).

For quantitative Western blot analysis based on band density, we performed double-immunoblotting using the anti-HtrA2/Omi antiserum and a mouse monoclonal anti-β-actin (Sigma, Saint Louis, MO, USA). After incubation with the combination of the anti-HtrA2/Omi (1:2000) plus the anti-β-actin (1:2000) antibody, membranes from the control, SALS and FALS cases were reacted with both alkaline phosphatase-labelled anti-rabbit IgG (1:1000) and anti-mouse IgG (Vector Laboratories, 1:1000). We measured the density of HtrA2/Omi-immunopositive and β-actin-immunopositive bands using LAS-3000 (Fujifilm, Tokyo, Japan), and calculated the percentage of the density of HtrA2/Omi-positive band based on the density of β-actin-positive band in each membrane.

Results

Western blot analysis

In the normal, SALS and FALS spinal cord homogenates, the anti-HtrA2/Omi antiserum immunostained a single band at a molecular weight of approximately 36 kDa (Figure 1A), which corresponded to the molecular weight of the mature form of human HtrA2/Omi. Our previous and present results indicated that the antiserum recog-

nized the mature form of HtrA2/Omi in human spinal cords as well as human brains [25].

As shown in Figure 1B, HtrA2/Omi-immunopositive and β-actin-immunopositive bands were detected in the double-immunostained membranes. The percentages of the density of HtrA2/Omi-positive band bases on the density of β-actin-positive band in the control, SALS and FALS spinal cord homogenates were 68.4%, 69.7% and 66.7%, respectively.

HtrA2/Omi immunoreactivity in normal and SALS spinal cords

In the anterior horn from the control subjects, mild-to-moderate HtrA2/Omi immunoreactivity was observed in the somata and proximal processes of the motor neurones (Figure 2A). A similar immunolabelling pattern was found in most of the remaining anterior horn cells from the patients with SALS (Figure 2B), but immunoreactive products accumulated densely in some surviving spinal motor neurones from the SALS cases (Figure 2C). In addition, in the anterior horn from the patients with SALS, many spheroids were intensely immunostained (Figure 2D), and some skein-like inclusions (SLIs) were immunopositive for HtrA2/Omi (Figure 2E). The RHIs, which were spherical eosinophilic structures (Figure 3A), were also immunolabelled (Figures 2F,3B), but the Bunina bodies, which were small eosinophilic structures (Figure 3C), were immunonegative for HtrA2/Omi (Figure 3D). HtrA2/Omi-immunopositive intracytoplasmic inclusions were observed in some remaining neurones in the globus pallidus and thalamus from the SALS case (SALS 11, data not shown).

HtrA2/Omi immunoreactivity in FALS spinal cords

Similar to the SALS cases, most of the remaining anterior horn cells were immunostained mildly to moderately in the FALS cases. The most conspicuous finding in the patients with FALS was the localization of HtrA2/Omi immunoreactivity in the LBHIs and CIs in the remaining anterior horn cells. In the patient with an Ala4Val mutation in the SOD1 gene, neuronal intracytoplasmic LBHIs (Figure 4A) and cord-like swollen neurites (Figure 4B) were intensely immunolabelled. In the patient with an Ile112Thr mutation in the SOD1 gene, neuronal intracytoplasmic LBHIs, which consisted of eosinophilic cores
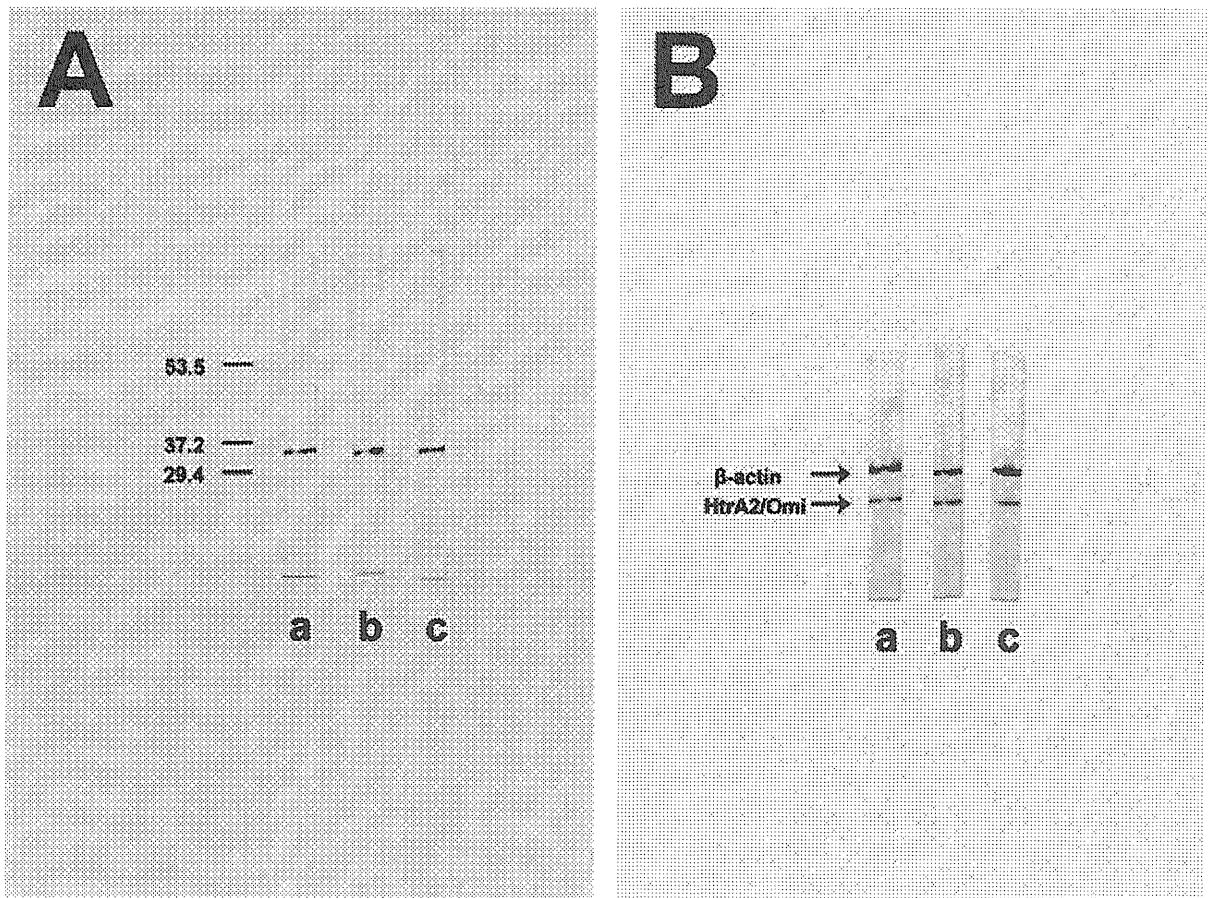
Figure 1. Western blot analysis of spinal cord homogenates from normal control (Aa, Ba), sporadic amyotrophic lateral sclerosis (Ab, Bb) and familial amyotrophic lateral sclerosis cases (Ac, Bc). Membranes were treated with the anti-HtrA2/Omi antiserum, and molecular weights are shown to the left in kDa (A). A single band at a molecular weight of approximately 36 kDa was detected in three types of membranes (A). Membranes were treated with the combination of the anti-HtrA2/Omi antiserum plus the anti-β-actin antibody (B). Both HtrA2/Omi- and β-actin-immunopositive bands were detected in three types of membranes (B).

and pale halos (Figure 5A), were densely immunostained (Figures 4C,5B). Strongly immunopositive LBHIs were also observed in the neuronal processes of the same case (Figure 4D). In the patient with a 2-base pair deletion at codon 126 in the SOD1 gene, neuronal intracytoplasmic LBHIs were heavily immunoreactive for HtrA2/Omi (Figure 4E). In the patient with an Ile113Thr mutation in the SOD1 gene, many CIs, which were pale eosinophilic structures (Figure 5C), were intensely immunostained (Figures 4F,5D).

Double-labelling immunohistochemistry for HtrA2/Omi and ubiquitin, TDP-43 or SOD1

The double-immunostained sections showed that HtrA2/Omi and ubiquitin or TDP-43 were co-localized in some

RHIs (Figure 6A–C) and SLIs (Figure 6D–F) in the remaining anterior horn cells from the patients with SALS. The co-localization of HtrA2/Omi and SOD1 was also observed in many LBHIs in the surviving spinal motor neurones from the patients with FALS (Figure 6G–I). The average percentages of HtrA2/Omi-immunopositive RHIs and LBHIs were 61.1% and 83.3%, respectively.

Discussion

In the present study, we performed immunohistochemical studies on HtrA2/Omi using autopsied human spinal cords from normal subjects and patients with ALS. To the best of our knowledge, this is the first report that demonstrates the immunohistochemical localization of HtrA2/
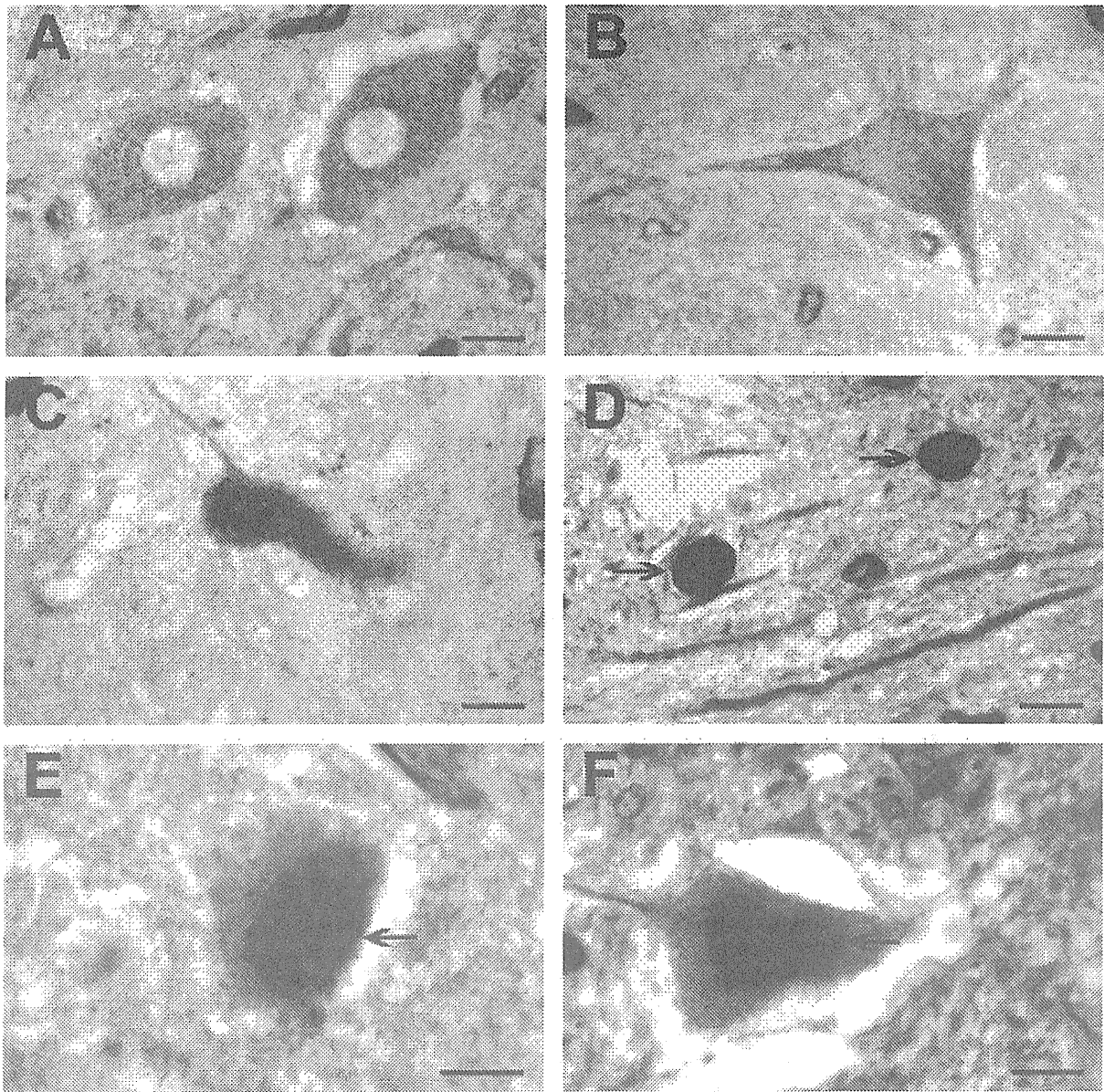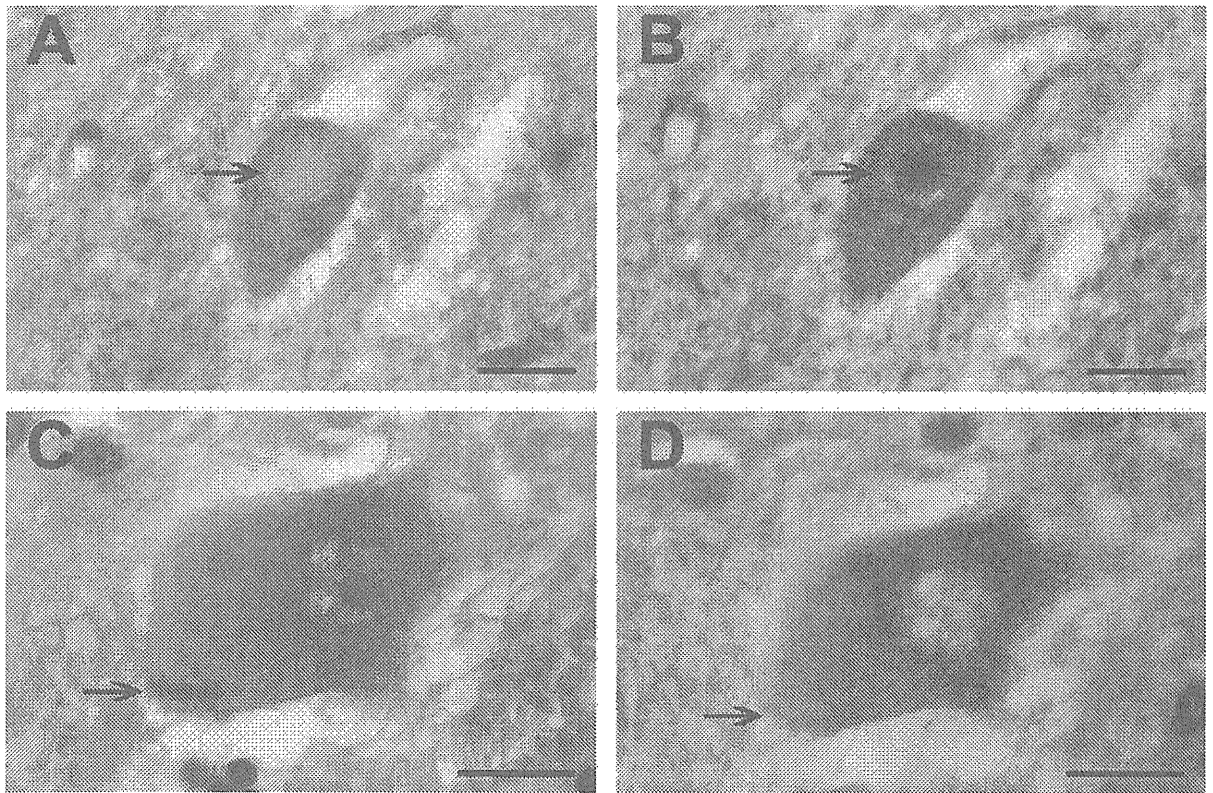
Figure 2. Lumbar spinal cord sections immunostained with the anti-HtrA2/Omi antiserum from normal control subjects (A: control 3) and patients with sporadic amyotrophic lateral sclerosis (SALS) (B: SALS 4; C,D: SALS 2; E: SALS 5; F: SALS 7). The anterior horn cells in the control cases (A) and normal-appearing motor neurones in the SALS cases (B) were mildly immunostained. Strong HtrA2/Omi immunoreactivity was observed in the atrophic motor neurones (C), spheroids (D, arrows), skein-like inclusions (E, arrow) and round hyaline inclusions (F, arrow) in the SALS cases. Scale bars = 20 μm.

Omi in several types of motor neuronal inclusions in the anterior horn from SALS and FALS cases. In the patients with SALS, we observed strong HtrA2/Omi immunoreactivity in some SLIs and RHIs as well as many spheroids. In the patients with SOD1-related FALS, we found that LBHIs, cord-like swollen neurites and CIs were intensely

immunostained with HtrA2/Omi. Our results suggest that abnormal accumulations of HtrA2/Omi may occur in the remaining anterior horn cells in both SALS and FALS cases.

Lewy body-like hyaline inclusions in general have eosinophilic cores surrounded by pale halos [3].
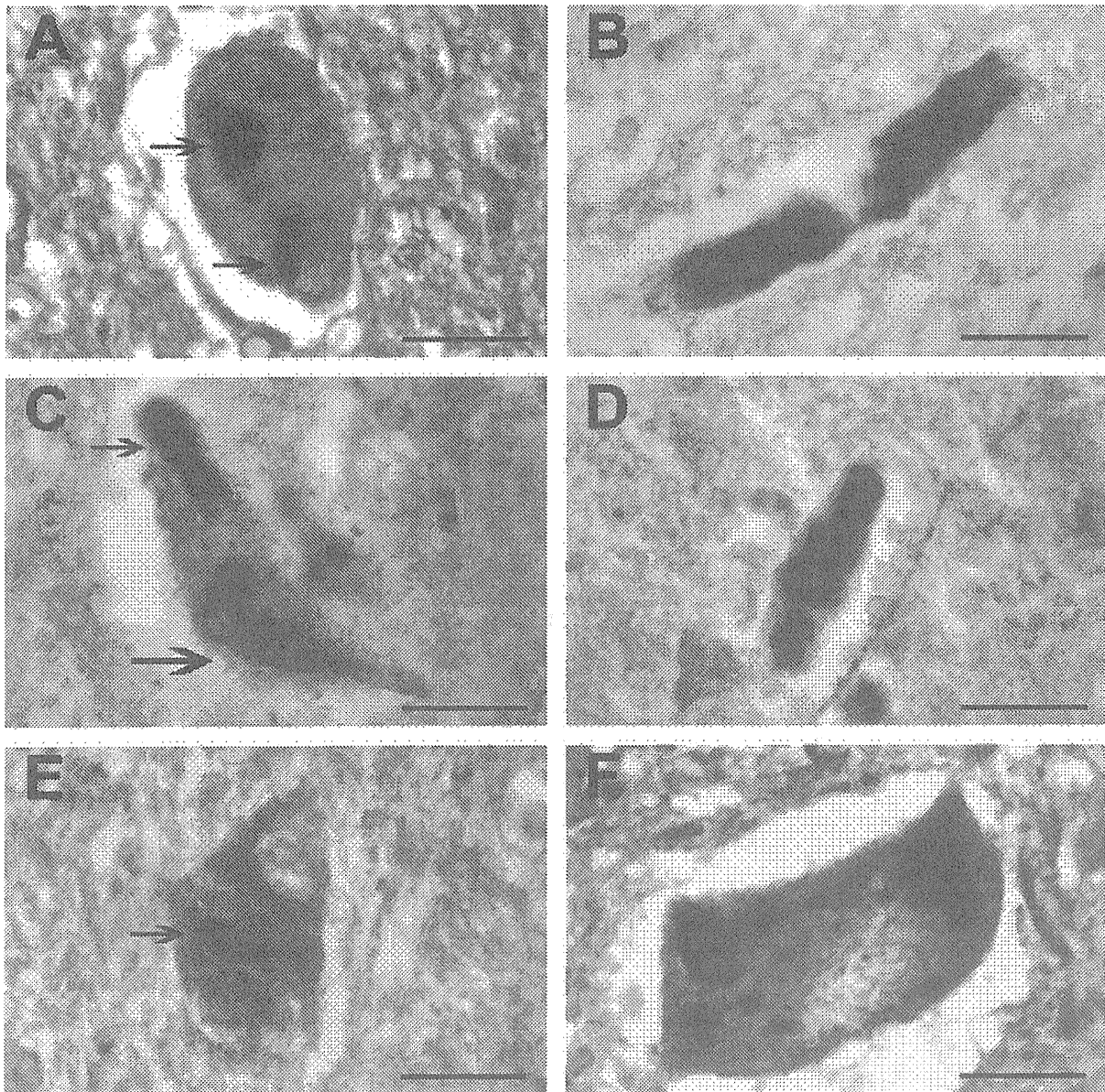
Figure 3. Lumbar spinal cord sections stained with haematoxylin and eosin (A: SALS 5; C: SALS 1) and immunostained with the anti-HtrA2/Omi antiserum (B: SALS 5; D: SALS 1). The round hyaline inclusion, which was identified by haematoxylin and eosin staining (A, arrow), was immunopositive for HtrA2/Omi (B, arrow), and A and B were the same section. The Bunina bodies, which were present in a cluster (C, arrow), were immunonegative for HtrA2/Omi (D, arrow), and C and D were the same section. Scale bars = 20 μm. SALS, sporadic amyotrophic lateral sclerosis.

Ultrastructurally, the core consists of granule-associated filaments and the halo is composed of normal-looking neurofilaments [26,27]. On the other hand, CIs are large argyrophilic inclusions that are frequently observed in FALS patients with an Ile113Thr mutation in the SOD1 gene [22–24]. On electron microscopy, CIs consist of massive accumulations of redundant neurofilaments [22,24]. Phosphorylated neurofilament immunoreactivity is mainly localized to the marginal zones of LBHIs [4], but CIs are diffusely immunopositive for both phosphorylated and non-phosphorylated neurofilaments [22–24]. In contrast to the ubiquitination of LBHIs [4,27], CIs generally show no or weak immunoreactivity for ubiquitin [23,24]. These data indicate that LBHIs are different from CIs ultrastructurally and immunohistochemically. In the present study, we detected strong HtrA2/Omi immunoreactivity in LBHIs and CIs, and our findings suggest that there may be a common process of

formation between LBHIs and CIs, and that HtrA2/Omi may make a partial contribution to the formation of both types of inclusions.

Mitochondrial abnormalities were reported in cultured cell lines expressing mutant human SOD1 [28,29] and in spinal cords from mSOD1-Tg mice [30,31]. These *in vitro* and *in vivo* data suggest that mitochondrial dysfunction may be associated with the pathogenesis of SOD1-related FALS. Mitochondrial dysfunction can, in turn, trigger apoptotic cell death. In fact, the release of cytochrome *c* from the mitochondria and the activation of several caspases, including caspase-9, have been demonstrated in spinal cords from mSOD1-Tg mice [18,32], suggesting that mitochondria-dependent cell death pathways may play an important role in motor neuronal degeneration in spinal cords from mSOD1-Tg mice. In the present study, we found intense HtrA2/Omi immunoreactivity in LBHIs, cord-like swollen neurites and CIs from four patients with
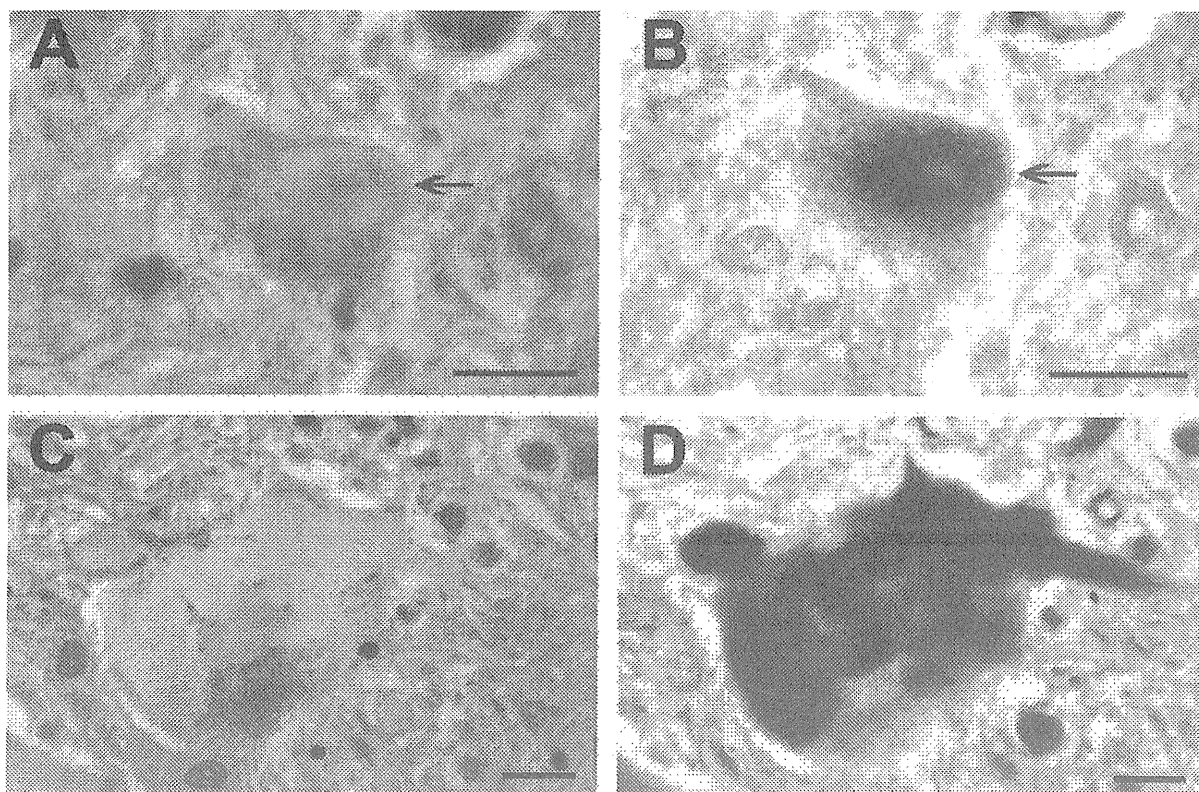
Figure 4. Lumbar spinal cord sections immunostained with the anti-HtrA2/Omi from patients with familial amyotrophic lateral sclerosis (A,B: FALS 1; C,D: FALS 2; E: FALS 3; F: FALS 4). In a patient with an Ala4Val mutation in the superoxide dismutase (SOD1) gene, strong HtrA2/Omi immunoreactivity was observed in irregularly shaped Lewy body-like hyaline inclusions (LBHIs) (A, arrows) and cord-like swollen neurites (B). In a patient with an Ile112Thr mutation in the SOD1 mutation, LBHIs in the neuronal cell bodies (C, small arrow) and processes (D) were intensely immunostained. Increased HtrA2/Omi immunoreactivity was found in the cytoplasm of LBHI-bearing motor neurones (C, large arrow). In a patient with a 2-base pair deletion at codon 126 in the SOD1 gene, neuronal intracytoplasmic LBHIs were densely immunolabelled (E, arrow). In a patient with an Ile113Thr mutation in the SOD1 gene, strongly immunoreactive conglomerate inclusions were observed in the somata of the surviving spinal motor neurones (F). Scale bars = 20 μm.

SOD1-related FALS. Our results suggest that HtrA2/Omi may accumulate in the abnormal structures characteristic for SOD1-linked FALS, and that mitochondria-dependent apoptotic processes may be involved in spinal motor neuronal degeneration in SOD1-related FALS patients as well as mSOD1-Tg mice.

Spheroids, LBHIs, cord-like swollen neurites and CIs are pathological structures that contain abundant

Figure 5. Lumbar spinal cord sections stained with haematoxylin and eosin (A: FALS 2; C: FALS 4) and immunostained with the anti-HtrA2/Omi antiserum (B: FALS 2; D: FALS 4). The Lewy body-like hyaline inclusion, which was identified by haematoxylin and eosin staining (A, arrow), was intensely immunostained (B, arrow), and A and B were the same section. The conglomerate inclusions, which were pale eosinophilic and multifocal large inclusions (C), were strongly immunopositive for HtrA2/Omi (D), and C and D were the same section. Scale bars = 20 μm. FALS, familial amyotrophic lateral sclerosis.

neurofilaments in patients with ALS. Proximal axonal enlargements are called 'spheroids', and many spheroids are often observed in the anterior horn from patients with ALS [33]. Our immunohistochemical study demonstrated that strong HtrA2/Omi immunoreactivity was localized to spheroids, LBHIs, cord-like swollen neurites and CIs, suggesting that HtrA2/Omi may be associated with abnormal accumulations of neurofilaments in the anterior horn from patients with ALS. Ultrastructurally, spheroids, LBHIs and dystrophic neurites contain some mitochondria as well as abundant neurofilaments [26,27,34]. In particular, CIs are closely related to neurofilamentous accumulations, and electron microscopic examinations have revealed that most intracellular organelles were displaced by large conglomerates of neurofilaments in the cytoplasm of CIs-containing upper and lower motor neurones [22,24,34]. Because CIs contain no or very few mitochondria, diffuse and robust HtrA2/Omi immunola-

belling patterns of CIs suggest that CIs may contain HtrA2/Omi released from the mitochondria, and that extramitochondrial HtrA2/Omi may play an important role in abnormal accumulations of neurofilaments.

Ubiquitin-positive neuronal cytoplasmic inclusions are a pathological hallmark of ALS [35–37]. TDP-43 was identified as a component of ubiquitinated inclusions in SALS and frontotemporal lobar degeneration [38,39], and these diseases are now collectively referred to as 'TDP-43 proteinopathy' [40]. SLIs and RHIs are intensely immunostained with TDP-43 in patients with SALS [38,39,41], but LBHIs are immunonegative for TDP-43 in patients with SOD1-related FALS [41]. On the other hand, RHIs, which are similar to LBHIs in morphology, are not immunolabelled with SOD1 [42]. These data indicate that the pathogenesis of SALS is different from that of SOD1-related FALS. In the present study, we observed that some SLIs and RHIs as well as many spheroids were densely
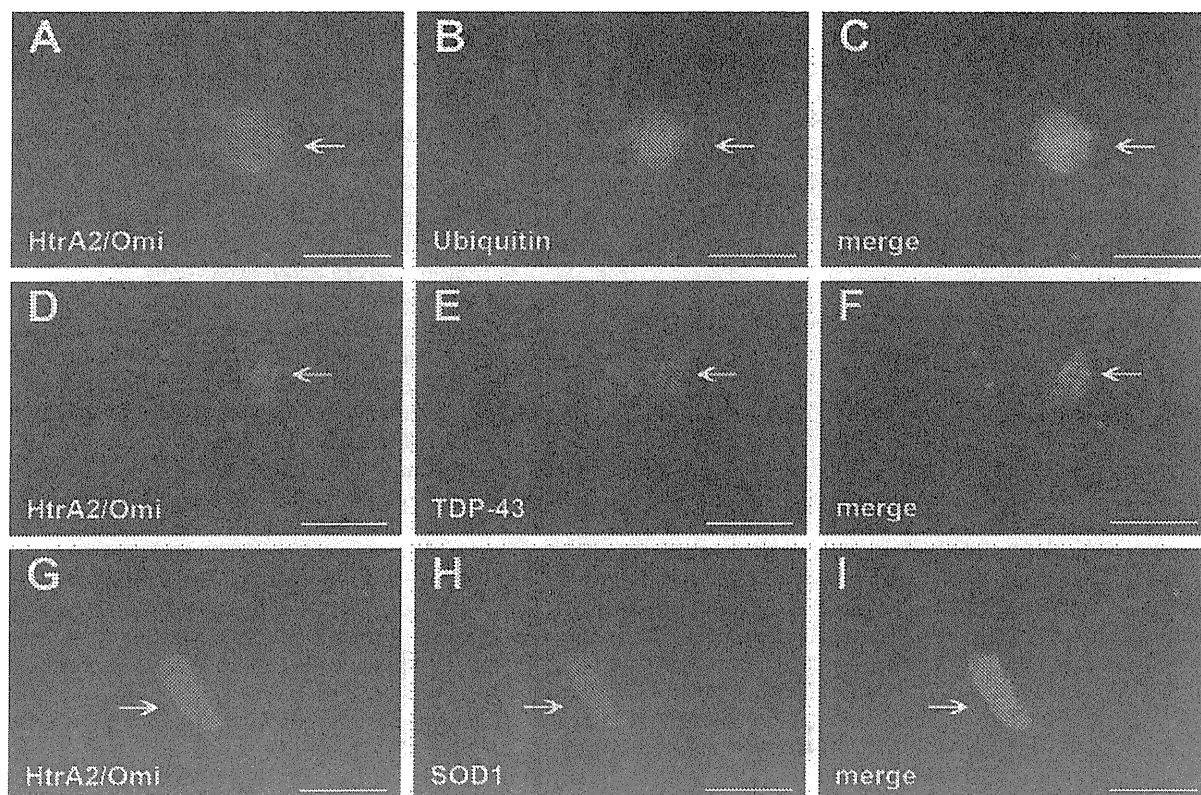
Figure 6. Double immunofluorescence staining of lumbar spinal cords for HtrA2/Omi (A: SALS 7; D: SALS 6; G: FALS 1), ubiquitin (B: SALS 7), TDP-43 (E: SALS 6) and SOD1 (H: FALS 1). The merged images (C: SALS 7; F: SALS 6; I: ALS 1) showed that HtrA2/Omi were localized in the ubiquitin-positive round hyaline inclusion (A–C, arrows), TDP-43-positive skein-like inclusions (D–F, arrows) and Lewy body-like hyaline inclusion (G–I, arrows). Scale bars = 20 μm. SALS, sporadic amyotrophic lateral sclerosis; FALS, familial amyotrophic lateral sclerosis; SOD1, Cu/Zn superoxide dismutase.

immunoreactive for HtrA2/Omi in patients with SALS. Furthermore, the translocation of cytochrome *c* and the activation of caspase-9 were immunohistochemically confirmed to occur in the anterior horn from patients with SALS [18,19]. These results suggest that mitochondria-dependent apoptotic processes may be involved not only in FALS, but also in SALS. On the other hand, several data have suggested the involvement of endoplasmic reticulum (ER) stress in sporadic [43–45] and SOD1-related FALS [45–47]. Because of the partial localization of HtrA2/Omi in the ER membranes [48], there is a possibility that HtrA2/Omi may be associated with ER stress in both types of ALS.

In conclusion, we found the enhanced immunoexpression of HtrA2/Omi in the anterior horn from SALS and SOD1-related FALS cases, suggesting that HtrA2/Omi may be associated with the pathogenesis of both types of

ALS. The close relationship between HtrA2/Omi and Parkinson's disease has been supported by several findings [49–52], and HtrA2/Omi is now designated as 'PARK13' [51,52]. Recently, we reported the immunohistochemical localization of HtrA2/Omi in alpha-synuclein-containing inclusions in Parkinson's disease, dementia with Lewy bodies, and multiple system atrophy [25]. These data suggest that HtrA2/Omi may play an important role in the pathogenesis of various types of neurodegenerative diseases, and that HtrA2/Omi may be one of the key proteins, which help us to understand the underlying mechanisms for mitochondria-related apoptosis in ALS and other neurodegenerative disorders. Of course, we cannot exclude a possibility that cytosolic release of HtrA2/Omi may simply reflect a common final pathway of cell death in several neurodegenerative disorders, including ALS and Parkinson's disease.

Acknowledgements

References

1 Gros-Louis F, Gaspar C, Rouleau GA. Genetics of familial and sporadic amyotrophic lateral sclerosis. *Biochem Biophys Acta* 2006; **1762**: 956–72

2 Rosen DR, Siddique T, Patterson D, Figlewicz DA, Sapp P, Hentati A, Donaldson D. Goto J, O'Regan JP, Deng H-X, Rahmani Z, Krizus A, McKenna-Yasek D, Cayabyab A, Gaston SM, Berger R, Tanzi RE, Halperin JJ, Herzfeldt B, Van den Bergh R, Hung W-Y, Bird T, Deng G, Mulder DW, Smyth C, Laing NG, Soriano E, Pericak-Vance MA, Haines J, Rouleau GA, Gusella JS, Horvitz HR, Brown Jr RH. Mutations in Cu/Zn superoxide dismutase gene are associated with familial amyotrophic lateral sclerosis. *Nature* 1993; **362**: 59–62

3 Hirano A, Kurland LT, Sayre GP. Familial amyotrophic lateral sclerosis: a subgroup characterized by posterior and spinocerebellar tract involvement and hyaline inclusions in the anterior horn cells. *Arch Neurol* 1967; **16**: 232–43

4 Shibata N, Hirano A, Kobayashi M, Siddique T, Deng H-X, Hung W-Y, Kato T, Asayama K. Intense superoxide dismutase-1 immunoreactivity in intracytoplasmic hyaline inclusions of familial amyotrophic lateral sclerosis with posterior column involvement. *J Neuropathol Exp Neurol* 1996; **55**: 481–90

5 Gurney ME, Pu H, Chiu AY, Canto MCD, Polchow CY, Alexander DD, Caliendo J, Hentati A, Kwon YW, Deng H-X, Chen W, Zhai P, Sufit RL, Siddique T. Motor neuron degeneration in mice that express a human Cu,Zn superoxide dismutase mutation. *Science* 1994; **264**: 1772–5

6 Li P, Nijhawan D, Budihardjo I, Srinivasula SM, Ahmad M, Alnemri ES, Wang X. Cytochrome c and dATP-dependent formation of Apaf-1/caspase-9 complex initiates an apoptotic protease cascade. *Cell* 1997; **91**: 479–89

7 Srinivasula SM, Ahmad M, Fernandes-Alnemri T, Alnemri ES. Autoactivation of procaspase-9 by Apaf-1-mediated oligomerization. *Mol Cell* 1998; **1**: 949–57

8 Deveraux QL, Takahashi R, Salvesen GS, Reed JC. X-linked IAP is a direct inhibitor of cell-death proteases. *Nature* 1997; **388**: 300–4

9 Takahashi R, Deveraux QL, Tamm I, Welsh K, Assa-Munt N, Salvesen GS, Reed JC. A single BIR domain of XIAP sufficient for inhibiting caspases. *J Biol Chem* 1998; **273**: 7787–90

10 Deveraux QL, Reed JC. IAP family proteins – suppressors of apoptosis. *Genes Dev* 1999; **13**: 239–52

11 Suzuki Y, Imai Y, Nakayama H, Takahashi K, Takio K, Takahashi R. A serine protease, HtrA2, is released from the mitochondria and interacts with XIAP, inducing cell death. *Mol Cell* 2001; **8**: 613–21

12 Hegde R, Srinivasula SM, Zhang Z, Wassell R, Mukattash R, Cilenti L, DuBois G, Lazebnik Y, Zervos AS, Fernandes-Alnemri T, Alnemri ES. Identification of Omi/HtrA2 as a mitochondrial apoptotic serine protease that disrupts inhibitor of apoptosis protein-caspase interaction. *J Biol Chem* 2002; **277**: 432–8

13 Martins LM, Iaccarino I, Tenev T, Gschmeissner S, Totty NF, Lemoine NR, Savopoulos J, Gray CW, Creasy CL, Dingwall C, Downward J. The serine protease Omi/HtrA2 regulates apoptosis by binding XIAP through a Reaper-like motif. *J Biol Chem* 2002; **277**: 439–44

14 Verhagen AM, Silke J, Ekert PG, Pakusch M, Kaufmann H, Connolly LM, Day CL, Tikoo A, Burke R, Wrobel C, Moritz RL, Simpson RJ, Vaux DL. HtrA2 promotes cell death through its serine protease activity and its ability to antagonize inhibitor of apoptosis proteins. *J Biol Chem* 2002; **277**: 445–54

15 Srinivasula SM, Gupta S, Datta P, Zhang Z, Hegde R, Cheong N, Fernandes-Alnemri T, Alnemri ES. Inhibitor of apoptosis proteins are substrates for the mitochondrial serine protease Omi/HtrA2. *J Biol Chem* 2003; **278**: 31469–72

16 Yang Q-H, Church-Hajduk R, Ren J, Newton ML, Du C. Omi/HtrA2 catalytic cleavage of inhibitor of apoptosis (IAP) irreversibly inactivates IAPs and facilitates caspase activity in apoptosis. *Genes Dev* 2003; **17**: 1487–96

17 Suzuki Y, Takahashi-Niki K, Akagi T, Hashikawa T, Takahashi R. Mitochondrial protease Omi/HtrA2 enhances caspase activation through multiple pathways. *Cell Death Differ* 2004; **11**: 208–16

18 Guégan C, Vila M, Rosoklija G, Hays AP, Przedborski S. Recruitment of the mitochondrial-dependent apoptotic pathways in amyotrophic lateral sclerosis. *J Neurosci* 2001; **21**: 6569–76

19 Inoue H, Tsukita K, Iwasato T, Suzuki Y, Tomioka M, Tateno M, Nagao M, Kawata A, Saido TC, Miura M, Misawa H, Itohara S, Takahashi R. The crucial role of caspase-9 in the disease progression of a transgenic ALS mouse model. *EMBO J* 2003; **22**: 6665–74

20 Kadekawa J, Fujimura H, Ogawa Y, Hattori N, Kaido M, Nishimura T, Yoshikawa H, Shirahata N, Sakoda S, Yanagihara T. A clinicopathological study of a patient with familial amyotrophic lateral sclerosis associated with a two base pair deletion in the copper/zinc superoxide dismutase (SOD1) gene. *Acta Neuropathol (Berl)* 1997; **94**: 617–22

21 Kadekawa J, Fujimura H, Yanagihara T, Sakoda S. A clinicopathological study of a patient with familial amyotrophic lateral sclerosis associated with a two-base pair deletion in the copper/zinc superoxide dismutase (SOD1) gene. *Acta Neuropathol (Berl)* 2001; 101: 415

22 Rouleau GA, Clark AW, Rooke K, Pramatarova A, Krizus A, Suchowersky O, Julien J-P, Figlewicz D. SOD1 mutation is associated with accumulation of neurofilaments in amyotrophic lateral sclerosis. *Ann Neurol* 1996; 39: 128–31

23 Ince PG, Tomkins J, Slade JY, Thatcher NM, Shaw PJ. Amyotrophic lateral sclerosis associated with genetic abnormalities in the gene encoding Cu/Zn superoxide dismutase: molecular pathology of five new cases, and comparison with previous reports and 73 sporadic cases of ALS. *J Neuropathol Exp Neurol* 1998; 57: 895–904

24 Kokubo Y, Kuzuhara S, Narita Y, Kikugawa K, Nakano R, Inuzuka T, Tsuji S, Watanabe M, Miyazaki T, Murayama S, Ihara Y. Accumulation of neurofilaments and SOD1-immunoreactive products in a patient with familial amyotrophic lateral sclerosis with I113T SOD1 mutation. *Arch Neurol* 1999; 56: 1506–8

25 Kawamoto Y, Kobayashi Y, Suzuki Y, Inoue H, Tomimoto H, Akiguchi I, Buduka H, Martins LM, Downward J, Takahashi R. Accumulation of HtrA2/Omi in neuronal and glial inclusions in brains with α-synucleinopathies. *J Neuropathol Exp Neurol* 2008; 67: 984–93

26 Hirano A, Nakano I, Kurland LT, Mulder DW, Holley PW, Saccomanno G. Fine structural study of neurofibrillary changes in a family with amyotrophic lateral sclerosis. *J Neuropathol Exp Neurol* 1984; 43: 471–80

27 Murayama S, Ookawa Y, Mori H, Nakano I, Ihara Y, Kuzuhara S, Tomonaga M. Immunocytochemical and ultrastructural study of Lewy body-like hyaline inclusions in familial amyotrophic lateral sclerosis. *Acta Neuropathol (Berl)* 1989; 78: 143–52

28 Carrì MT, Ferri A, Battistoni A, Famhy L, Gabbianelli R, Poccia F, Rotilio G. Expression of a Cu,Zn superoxide dismutase typical of familial amyotrophic lateral sclerosis induces mitochondrial alteration and increase of cytosolic Ca^{2+} concentration in transfected neuroblastoma SH-SY5Y cells. *FEBS Lett* 1997; 414: 365–8

29 Menzies FM, Cookson MR, Taylor RW, Turnbull DM, Chrzanowska-Lightowlers ZMA, Dong L, Figlewicz DA, Shaw PJ. Mitochondrial dysfunction in a cell culture model of familial amyotrophic lateral sclerosis. *Brain* 2002; 125: 1522–33

30 Wong PC, Pardo CA, Borchelt DR, Lee MK, Copeland NG, Jenkins NA, Sisodia SS, Cleveland DW, Price DL. An adverse property of a familial ALS-linked SOD1 mutation causes motor neuron disease characterized by vacuolar degeneration of mitochondria. *Neuron* 1995; 14: 1105–16

31 Kong J, Xu Z. Massive mitochondrial degeneration in motor neurons triggers the onset of amyotrophic lateral sclerosis in mice expressing a mutant SOD1. *J Neurosci* 1998; 18: 3241–50

32 Li M, Ona VO, Guégan C, Chen M, Jackson-Lewis V, Andrews LJ, Olszewski AJ, Stieg PE, Lee J-P, Przedborski S, Friedlander RM. Functional role of caspase-1 and caspase-3 in an ALS transgenic mouse model. *Science* 2000; 288: 335–9

33 Carpenter S. Proximal axonal enlargement in motor neuron disease. *Neurology* 1968; 18: 841–51

34 Chou SM, Wang HS, Taniguchi A. Role of SOD-1 and nitric oxide/cyclic GMP cascade on neurofilament aggregation in ALS/MND. *J Neurol Sci* 1996; 139: 16–26

35 Leigh PN, Anderton BH, Dodson A, Gallo J-M, Swash M, Power DM. Ubiquitin deposits in anterior horn cells in motor neuron disease. *Neurosci Lett* 1988; 93: 197–203

36 Lowe J, Lennox G, Jefferson D, Morrell K, McQuire D, Gray T, Landon M, Doherty FJ, Mayer RJ. A filamentous inclusion body within anterior horn neurons in motor neuron disease defined by immunocytochemical localization of ubiquitin. *Neurosci Lett* 1988; 94: 203–10

37 Migheli A, Attanasio A, Schiffer D. Ubiquitin and neurofilament expression in anterior horn cells in amyotrophic lateral sclerosis: possible clues to the pathogenesis. *Neuropathol Apple Neurobiol* 1994; 20: 282–9

38 Neumann M, Sampathu DM, Kwong LK, Truax AC, Micsenyi MC, Chou TT, Bruce J, Schuck T, Grossman M, Clark CM, McCluskey LF, Miller BL, Masliah E, Mackenzie IR, Feldman H, Feiden W, Kretzschmar HA, Trojanowski JQ, Lee VM-Y. Ubiquitinated TDP-43 in frontotemporal lobar degeneration and amyotrophic lateral sclerosis. *Science* 2006; 314: 130–3

39 Arai T, Hasegawa M, Akiyama H, Ikeda K, Nonaka T, Mori H, Mann D, Tsuchiya K, Yoshida M, Hashizume Y, Oda T. TDP-43 is a component of ubiquitin-positive tau-negative inclusions in frontotemporal lobar degeneration and amyotrophic lateral sclerosis. *Biochem Biophys Res Commun* 2006; 351: 602–11

40 Geser F, Martinez-Lage M, Kwong LK, Lee VM-Y, Trojanowski JQ. Amyotrophic lateral sclerosis, frontotemporal dementia and beyond: the TDP-43 disease. *J Neurol* 2009; 256: 1205–14

41 Tan C-F, Eguchi H, Tagawa A, Onodera O, Iwasaki T, Tsujino A, Nishizawa M, Kakita A, Takahashi H. TDP-43 immunoreactivity in neuronal inclusions in familial amyotrophic lateral sclerosis with or without SOD1 gene mutation. *Acta Neuropathol (Berl)* 2007; 113: 535–42

42 Kato S, Takikawa M, Nakashima K, Hirano A, Cleveland DW, Kusaka H, Shibata N, Kato M, Nakano I, Ohama E. New consensus research on neuropathological aspects of familial amyotrophic lateral sclerosis with superoxide dismutase 1 (SOD1) gene mutations: inclusions containing SOD1 in neurons and astrocytes. *Amyotroph Lateral Scler Other Motor Neuron Disord* 2000; 1: 163–84

43 Ilieva EV, Ayala V, Jové M, Dalfó E, Cacabelos D, Povedano M, Bellmunt MJ, Ferrer I, Pamplona R, Portero-Otín M.

Oxidative and endoplasmic reticulum stress interplay in sporadic amyotrophic lateral sclerosis. *Brain* 2007; **130**: 3111–23

44 Oyanagi K, Yamazaki M, Takahashi H, Watabe K, Wada M, Komori T, Morita T, Mizutani T. Spinal anterior horn cells in sporadic amyotrophic lateral sclerosis show ribosomal detachment form, and cisternal distention of the rough endoplasmic reticulum. *Neuropathol Appl Neurobiol* 2008; **34**: 650–8

45 Kanekura K, Suzuki H, Aiso S, Matsuoka M. ER stress and unfolded protein response in amyotrophic lateral sclerosis. *Mol Neurobiol* 2009; **39**: 81–9

46 Kikuchi H, Almer G, Yamashita S, Guégan C, Nagai M, Xu Z, Sosunov AA, McKhann II GM, Przedborski S. Spinal cord endoplasmic reticulum stress associated with a microsomal accumulation of mutant superoxide dismutase-1 in an ALS model. *Proc Natl Acad Sci USA* 2006; **103**: 6025–30

47 Yamagishi S, Koyama Y, Katayama T, Taniguchi M, Hitomi J, Kato M, Aoki M, Itoyama Y, Kato S, Tohyama M. An in vitro model for Lewy body-like hyaline inclusions/astrocytic hyaline inclusion: induction by ER stress with an ALS-linked SOD1 mutation. *PloS One* 2007; **10**: e1030

48 Huttunen HJ, Guénette SY, Peach C, Greco C, Xia W, Kim DY, Barren C, Tanzi RE, Kovacs DM. HtrA2 regulates β-amyloid precursor protein (APP) metabolism through endoplasmic reticulum-associated degradation. *J Biol Chem* 2007; **282**: 28285–95

49 Martins LM, Morrison A, Klupsch K, Fedele V, Moisoi N, Teismann P, Abuin A, Grau E, Geppert M, Livi GP, Creasy CL, Martin A, Hargreaves I, Heales SJ, Okada H, Brandner S, Schulz JB, Mak T, Downward J. Neuroprotective role of the Reaper-related serine protease HtrA2/Omi revealed by targeted deletion in mice. *Mol Cell Biol* 2004; **24**: 9848–62

50 Strauss KM, Martins LM, Plun-Favreau H, Marx FP, Kautzmann S, Berg D, Gasser T, Wszolek Z, Müller T, Bornemann A, Wolburg H, Downward J, Riess O, Schulz JB, Krüger R. Loss of function mutations in the gene encoding Omi/HtrA2 in Parkinson's disease. *Hum Mol Genet* 2005; **14**: 2099–111

51 Plun-Favreau H, Klupsch K, Moisoi N, Gandhi S, Kjaer S, Frith D, Harvey K, Deas E, Harvey RJ, McDonald N, Wood NW, Martins LM, Downward J. The mitochondrial protease HtrA2 is regulated by Parkinson's disease-associated kinase PINK1. *Nat Cell Biol* 2007; **9**: 1243–52

52 Plun-Favreau H, Gandhi S, Wood-Kaczmar A, Deas E, Yao Z, Wood NW. What have PINK1 and HtrA2 genes told us about the role of mitochondria in Parkinson's disease? *Ann N Y Acad Sci* 2008; **1147**: 30–6

Stroke

American Stroke
Association.

A Division of American
Heart Association

The online version of this article, along with updated information and services, is
located on the World Wide Web at:
http://stroke.ahajournals.org/cgi/content/full/41/8/1798

Nonhypotensive Dose of Telmisartan Attenuates Cognitive Impairment Partially Due to Peroxisome Proliferator-Activated Receptor-γ Activation in Mice With Chronic Cerebral Hypoperfusion

Kazuo Washida, MD; Masafumi Ihara, MD; Keiko Nishio, MD; Youshi Fujita, MD;
Takakuni Maki, MD; Mahito Yamada, MD; Jun Takahashi, MD; Xiaofeng Wu, MS;
Takeshi Kihara, MD; Hidefumi Ito, MD; Hidekazu Tomimoto, MD; Ryosuke Takahashi, MD

Background and Purpose—The effect of telmisartan, an angiotensin II Type 1 receptor blocker with peroxisome proliferator-activated receptor-γ-modulating activity, was investigated against spatial working memory disturbances in mice subjected to chronic cerebral hypoperfusion.

Methods—Adult C57BL/6J male mice were subjected to bilateral common carotid artery stenosis using external microcoils. Mice received a daily oral administration of low-dose telmisartan (1 mg/kg per day), high-dose telmisartan (10 mg/kg per day), or vehicle with or without peroxisome proliferator-activated receptor-γ antagonist GW9662 (1 mg/kg per day) for all treatments for 30 days after bilateral common carotid artery stenosis. Cerebral mRNA expression of monocyte chemoattractant protein-1 and tumor necrosis factor-α was measured 30 days after bilateral common carotid artery stenosis, and postmortem brains were analyzed for demyelinating change with Klüver-Barrera staining and immunostained for glial, oxidative stress, and vascular endothelial cell markers. Spatial working memory was assessed by the Y-maze test.

Results—Mean systolic blood pressure and cerebral blood flow did not decrease with low-dose telmisartan but significantly decreased with high-dose telmisartan. Low-dose telmisartan significantly attenuated, but high-dose telmisartan provoked, spatial working memory impairment with glial activation, oligodendrocyte loss, and demyelinating change in the white matter. Such positive effects of low-dose telmisartan were partially offset by cotreatment with GW9662. Consistent with this, low-dose telmisartan reduced the degree of oxidative stress of vascular endothelial cells and the mRNA levels of monocyte chemoattractant protein-1 and tumor necrosis factor-α compared with vehicle.

Conclusions—Anti-inflammatory and antioxidative effects of telmisartan that were exerted in part by peroxisome proliferator-activated receptor-γ activation, but not its blood pressure-lowering effect, have protective roles against cognitive impairment and white matter damage after chronic cerebral hypoperfusion. (*Stroke*. 2010;41:1798-1806.)

Key Words: chronic cerebral hypoperfusion ■ oligovascular niche ■ oxidative stress ■ PPAR-γ ■ telmisartan

Drugs that target the renin–angiotensin system seem to have particular potential for prevention of dementias, including Alzheimer disease and vascular dementia. The Perindopril Protection Against Recurrent Stroke Study (PROGRESS) has suggested a protective effect of angiotensin-converting enzyme inhibitors on cognitive function in patients with stroke.[1] Moreover, the Study on Cognition and Prognosis in the Elderly (SCOPE) trial demonstrated a positive effect of the angiotensin II Type 1 receptor blocker (ARB), candesartan, in a subgroup of elderly hypertensive patients with mild cognitive impairment.[2] Notably, a prospective cohort analysis of 819 491 participants suggested that

ARBs are associated with a significant reduction in the incidence and progression of dementia, even compared with angiotensin-converting enzyme inhibitors.[3]

No benefit was found in cognitive performance after administration of the ARB, telmisartan, at the subacute stage (within 15 days) after stroke in the Prevention Regimen for Effectively Avoiding Second Strokes (PRoFESS) study.[4] However, in vitro studies have suggested that telmisartan, the strongest peroxisome proliferator-activated receptor-γ (PPAR-γ) activator among ARBs,[5] may protect oligodendrocytes and neurons through a reduction of brain inflammation through PPAR-γ activation and AT_1 receptor blockade.

Experimental Groups

Figure 1. Experimental protocol. Tel (Low) indicates low-dose telmisartan (1 mg/kg per day); Tel (High), high-dose telmisartan (10 mg/kg per day); GW, GW9662 (1 mg/kg per day); RT-PCR, reverse transcriptase–polymerase chain reaction.

Telmisartan has structural similarities to the PPAR-γ ligand pioglitazone and thus could act as a partial agonist of PPAR-γ.[5] PPAR-γ, one of the nuclear receptors, plays a critical role in a variety of biological processes, including angiogenesis, inflammation, oxidative stress, glucose metabolism, and adipogenesis.[5] Moreover, PPAR-γ activation in the brain has been suggested as a protective effect against Alzheimer disease through its multifaceted effects, including anti-inflammation and amyloid-β clearance.[6] Therefore, in the PRoFESS study, excessive lowering of blood pressure (BP) in the period with cerebrovascular autoregulatory dysfunction may have affected the cerebral circulation and neuronal function, although other factors could also be involved.

The present study is therefore designed to explore the multifaceted effects of telmisartan on cognitive disturbances in a mouse model of vascular dementia by administering a hypotensive or a nonhypotensive dose of telmisartan. This model of chronic cerebral hypoperfusion, which is produced by placing microcoils bilaterally on the common carotid arteries, invariably exhibits glial activation, oxidative stress, inflammation, demyelinating change, and axonal loss in the white matter with resultant spatial working memory deficits.[7,8] This in vivo system will help determine whether telmisartan affects vascular autoregulatory function and whether and how telmisartan exerts its protective effect against cognitive impairment related to white matter damage.

Materials and Methods

Experimental Protocol

The experimental protocol is shown in Figure 1. Nine-week-old male C57BL/6J mice (weighing 24 to 29 g; CLEA, Tokyo, Japan) were fed with the pelleted chow (MF) containing low-dose telmisartan (1 mg/kg per day), high-dose telmisartan (10 mg/kg per day), or vehicle with or without PPAR-γ antagonist GW9662 (1 mg/kg per day; Sigma-Aldrich) for all treatments, beginning from 7 days before the bilateral common carotid artery stenosis (BCAS) surgery until 30

days post-BCAS. Immediately after spatial working memory was assessed by the Y-maze test, mice were euthanized for histological and real-time reverse transcriptase–polymerase chain reaction examination 30 days post-BCAS.

Surgical Procedure of BCAS

Under anesthesia with halothane (2%), both common carotid arteries were exposed through a midline cervical incision, and a microcoil with an inner diameter of 0.18 mm was applied to the bilateral common carotid arteries. See Supplemental Method I for details (available at http://stroke.ahajournals.org).[7,8]

Systolic BP and Cerebral Blood Flow Measurements

Various doses of telmisartan (0 to 100 mg/kg per day) were administered and the BP measured for determining nonhypotensive and hypotensive doses of telmisartan. Then, in mice receiving the predetermined nonhypotensive or hypotensive dose of telmisartan or vehicle, systolic BP and cerebral blood flow (CBF) were monitored at 7 days before BCAS (before starting telmisartan treatment), immediately before BCAS, and 2 hours, 1 day, 3 days, 7 days, 14 days, and 30 days after BCAS. See Supplemental Method II for details.

Histochemical Evaluation of White Matter Lesions, Glial Activation, and Oxidative Stress

The mouse brains were analyzed for demyelinating change with Klüver-Barrera staining and immunostained for glial fibrillary acidic protein (a marker of astrocyte), ionized calcium binding adaptor molecule-1 (Iba-1; microglia), glutathione S-transferase-π (GST-π; oligodendrocyte), 8-hydroxy-deoxyguanosine (8-OHdG; oxidative stress), and CD31 (vascular endothelial cell). See Supplemental Method III for details.[7]

Quantitative Real-Time Reverse Transcriptase–Polymerase Chain Reaction

Cerebral mRNA levels of monocyte chemoattractant protein-1 (MCP-1) and tumor necrosis factor-α (TNF-α) were assessed by quantitative real-time reverse transcriptase–polymerase chain reaction pre-BCAS and 30 days post-BCAS. Detailed procedures are described in Supplemental Method IV.

Y-Maze Test for Spatial Working Memory Assessment

Spatial working memory was assessed by the Y-maze test. The detail of the Y-maze test protocol is described in Supplemental Method V.

Blood Concentration of Telmisartan

See Supplemental Method VI for details.

Statistical Analysis

All values are expressed as means±SEM in the text and figures. One-way analysis of variance was used to evaluate significant differences among groups except when otherwise stated. When a statistically significant effect was found, a post hoc Tukey test or Tukey-Kramer test was performed to detect the difference between the groups. Temporal profiles of systolic BP and CBF were analyzed by 2-way repeated-measures analysis of variance followed by a post hoc Tukey test. Differences with $P<0.05$ were considered statistically significant in all statistical analyses used.

Results

Systolic BP and CBF After Telmisartan Administration

Treatment with telmisartan, ≤ 1 mg/kg per day, did not result in a significant reduction in BP, whereas treatment with telmisartan ≥ 3 mg/kg per day resulted in a significant reduction in BP (Figure 2A). CBF was not significantly reduced ≤ 1 mg/kg per day but began to decrease at 3 mg/kg per day (Figure 2B). A nonhypotensive dose of 1 mg/kg per day or a hypotensive dose of 10 mg/kg per day was subsequently administered. Temporal profiles of systolic BP and CBF were not affected by administration of a nonhypotensive dose of telmisartan or addition of GW9662 (Figure 2C–E). CBF gradually recovered after BCAS in mice with vehicle or a nonhypotensive dose of telmisartan but not in those with a hypotensive dose of telmisartan (Figure 2E).

The mortality rates were 10% at ≤ 1 mg/kg per day in the telmisartan-treated group after BCAS surgery. The mortality rate increased to 30% at 3 mg/kg per day in the telmisartan-treated group and 50% at 10 mg/kg per day in the telmisartan-treated group. Eighty percent at 50 or 100 mg/kg per day in the telmisartan-treated group died within 3 days post-BCAS.

Effects of Telmisartan on Glial Activation, Oligodendrocyte Restoration, and White Matter Lesion in Mouse Brain With Chronic Cerebral Hypoperfusion

Immunohistochemical analysis showed that in response to ischemic insults, resting astrocytes and microglia appeared to enter a reactive state due to apparent morphological changes characterized by thick dendritic formation. Such morphological changes, however, were attenuated by a nonhypotensive dose of telmisartan (Figure 3; compare 3A and 3C and compare 3I and 3K). Both the number of glial fibrillary acidic protein-positive astrocytes and Iba-1-positive microglia were significantly reduced in both the corpus callosum and anterior commissure from a nonhypotensive dose of telmisartan-treated BCAS mice compared with the vehicle-treated BCAS mice (Figure 3G–H, O–P). Such effects of low-dose telmisartan were partially offset by cotreatment with GW9662 (Figure 3; compare 3C and 3D and compare 3K and 3L).

Next, a hypotensive dose of telmisartan was examined to assess whether it ameliorated glial activation in BCAS-treated mice. In contrast to a nonhypotensive dose, a hypotensive dose of telmisartan caused substantial glial activation in the white matter (Figure 3; compare 3C and 3E and compare 3K and 3M). Cotreatment with GW9662 did not lead to additional glial changes in the white matter of mice with vehicle (Figure 3; compare 3A and 3B and compare 3I and 3J) or high-dose telmisartan (Figure 3; compare 3E and 3F and compare 3M and 3N).

Klüver-Barrera staining showed that white matter lesions were significantly attenuated in the nonhypotensive group compared with the vehicle group (Figure 4; compare 4A and 4C). Although patterns in oligodendrocytes arrangement could not be seen in the vehicle-treated mice (Figure 4A), alignment in a row formation could be seen in the group given a nonhypotensive dose of telmisartan (Figure 4C). Such effects of low-dose telmisartan were also partially offset by GW9662 (Figure 4; compare 4C and 4D) with significant differences (Figure 4G–H). In contrast, high-dose telmisartan did not attenuate white matter lesions (Figure 4; compare 4A and 4E). There were no significant histological differences between vehicle and high-dose telmisartan-treated mice with or without GW9662. In addition, administration of GW9662 had no effects on morphology of the white matter in sham-operated mice (data not shown), vehicle-treated, BCAS-operated mice (Figure 4; compare 4A and 4B), and high-dose telmisartan-treated, BCAS-operated mice (Figure 4; compare 4E and 4F). White matter lesion Grade 3 (disappearance of myelinated fibers) was only partially (approximately 10% of the white matter) observed in mice with vehicle or high-dose telmisartan.

In addition, the number of GST-π-positive oligodendrocytes of the vehicle-treated mice were significantly decreased in the white matter compared with that of mice treated with a nonhypotensive dose of telmisartan (Figure 4I–K).

Telmisartan Attenuates mRNA Expression of Inflammatory Cytokines in Mouse Brain With Chronic Cerebral Hypoperfusion

Cerebral mRNA expression of inflammatory cytokines such as MCP-1 and TNF-α was significantly increased after the BCAS but significantly attenuated by a nonhypotensive dose of telmisartan 30 days post-BCAS (Figure 4L–M).

Vascular Endothelial Oxidative Stress in Mouse Brain With Chronic Cerebral Hypoperfusion Was Ameliorated by Telmisartan

To further explore the antioxidative effect of telmisartan, 8-OHdG-positive vascular endothelial cells of the brain were assessed. The number of CD31-positive vascular endothelial cells positive for 8-OHdG was markedly reduced by a nonhypotensive dose of telmisartan (Figure 5; compare 5A and 5C). The difference was statistically significant as assessed by 8-OHdG/CD31-positive area (%; the percentage of 8-OHdG-positive area to CD31-positive area; Figure 5J). Such antioxidative effects of low-dose telmisartan were partially offset by cotreatment with GW9662 (Figure 5; compare 5C and 5D). By contrast, high-dose telmisartan showed an attenuated antioxidative effect in comparison to low-dose telmisartan (Figure 5;
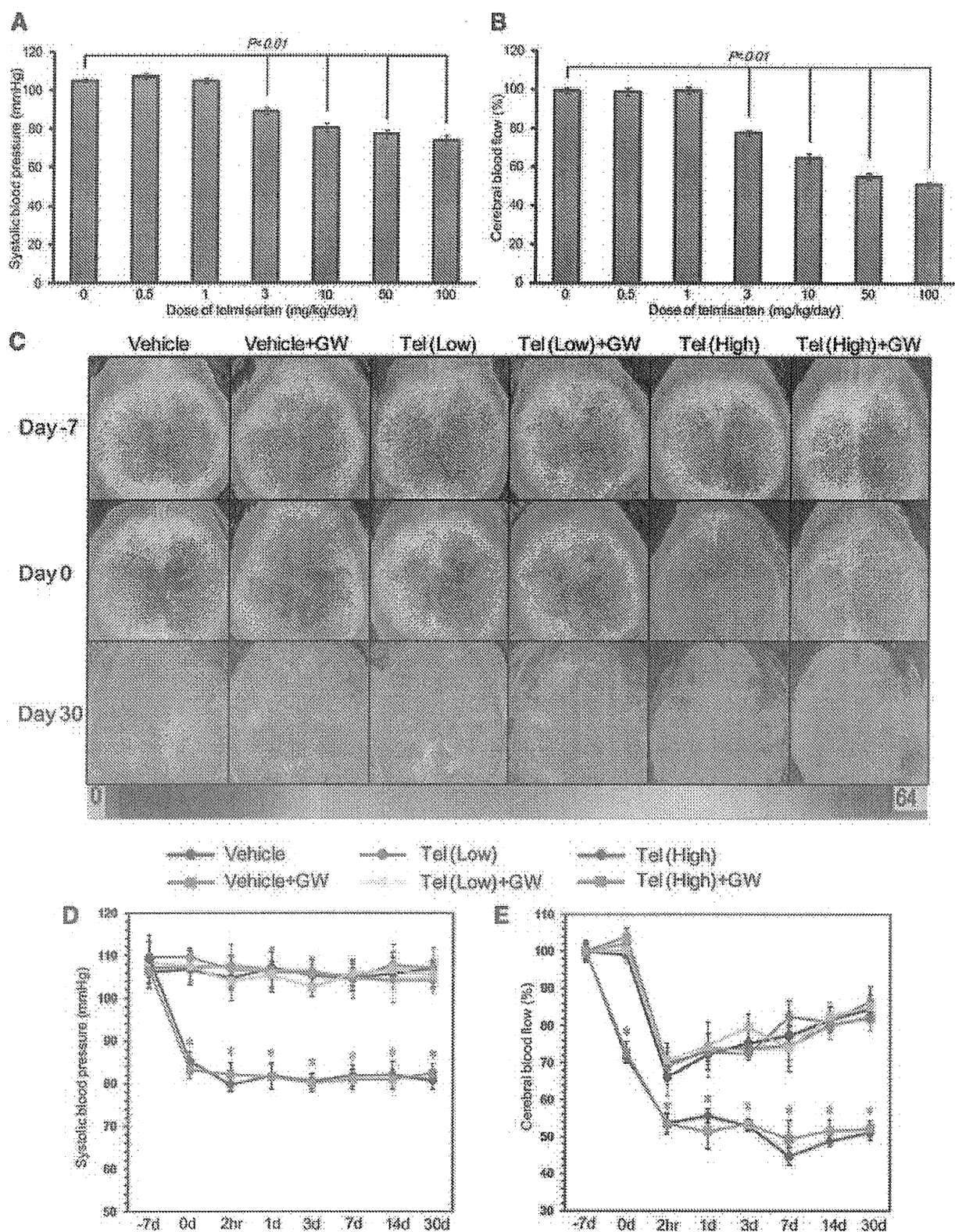
Figure 2. Systolic BP (A) and CBF (B) in mice treated with various doses of telmisartan (n=10 each). Representative CBF images of the 6 groups of mice as assessed by laser speckle flowmetry 7 days before (Day −7) and immediately before (Day 0) BCAS and 30 days post-BCAS (Day 30; C). Temporal profiles of systolic BP (D) and CBF (E) of the 6 groups of mice (n=5 each). CBF was expressed as a percentage of baseline flow. $F_{5,24}=84.100$ (D), $F_{5,24}=37.441$ (E), *$P<0.01$ versus vehicle.
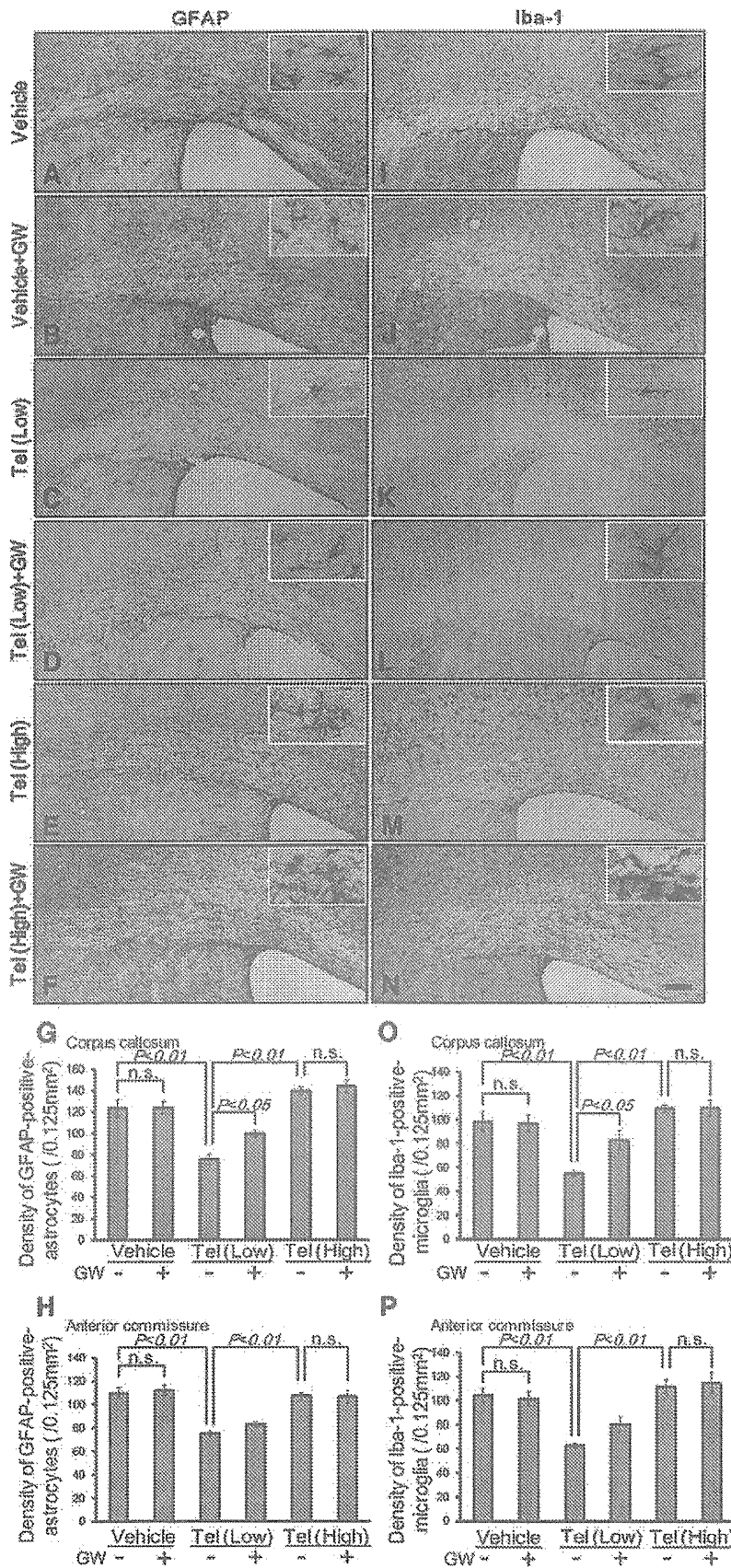
Figure 3. Representative images of immunohistochemistry for glial fibrillary acidic protein (GFAP; A–F) and Iba-1 (I–N) in the paramedian parts of the corpus callosum of the BCAS-operated mice treated with vehicle (A, I), vehicle+GW (B, J), Tel (Low; C, K), Tel (Low)+GW (D, L), Tel (High; E, M), and Tel (High)+GW (F, N) 30 days post-BCAS (n=7 each). Insets indicate enlarged images of astrocytes (A–F) and microglia (I–N). Scale bar, 100 μm. Histogram showing the density of GFAP-positive astrocytes (G–H) and Iba-1-positive microglia (O–P) in the corpus callosum (G, O) and anterior commissure (H, P) of the 6 groups of mice. Tel (Low) indicates low-dose telmisartan (1 mg/kg per day); Tel (High), high-dose telmisartan (10 mg/kg per day); GW, GW9662 (1 mg/kg per day).